# Accurate Numerical Modeling of Complex Thermal Processes: Impact of Professor Spalding's Work


**Yogesh Jaluria**

## 1 Introduction

Mathematical and numerical modeling of thermal processes that arise in important applications such as those related to energy, manufacturing, transportation, aerospace, heating, cooling, and the environment is crucial in a detailed study of the phenomena and in the design and optimization of the relevant systems. Most of these practical circumstances are too complicated to be investigated by analytical methods. Also, relatively limited data are usually available from existing processes and from experimental studies, which are often expensive and time consuming. Therefore, in most cases, mathematical models of the processes are developed and solved by numerical simulation. The models are validated by means of analytical and experimental results available on simpler and similar systems. Then, the numerical simulation is used to provide the extensive inputs needed for understanding and characterizing the processes, as well as for design, control, and optimization [1–3].

Practical thermal processes and systems typically involve complex, coupled, transport mechanisms and interacting components, and subsystems that constitute the overall system. Therefore, several challenges are commonly encountered in obtaining accurate results from the numerical simulation of these systems. Some of these are variable material properties, accurate and realistic imposition of boundary conditions, model validation, combined mechanisms, complex phenomena, multiple scales, multi-objective optimization, uncertainties, and other additional effects. This paper considers some of these aspects, presents examples where these considerations are important, and discusses possible approaches to meet these challenges. The work done by Professor Spalding and his group is indispensable in meeting many of the challenges discussed here. This will be pointed out at several places in this paper.

Y. Jaluria (✉)
Department of Mechanical & Aerospace Engineering,
Rutgers University, Piscataway, NJ 08854, USA
e-mail: jaluria@soe.rutgers.edu



A. Runchal (ed.), *50 Years of CFD in Engineering Sciences*,
https://doi.org/10.1007/978-981-15-2670-1_5

Professor Spalding contributed to a wide range of problems in heat and mass transfer and in fluid mechanics. Among the major areas that he contributed substantially to are the following:

- Combustion
- Multiphase transport
- Separated flows
- Turbulent flows
- Boundary layers; parabolic flows
- Recirculating flows
- Complex domains; grid generation; boundary conditions
- Complicated Practical Processes and Systems
- Computational Fluid Dynamics (CFD)
- Computer codes or programs such as Phoenics, Simple and Genmix

Clearly, he tackled some very complex problems and developed techniques to solve them through computational methods. This legacy has been of great importance to the fluids and heat transfer communities. His methods and basic approaches to various problems have paved the way to the solution of many challenging problems today.

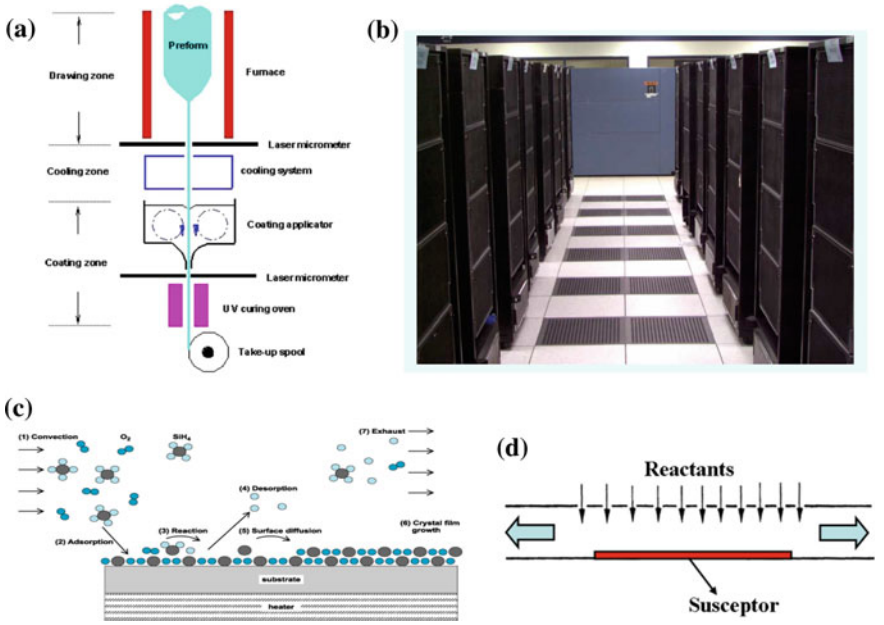


**Fig. 1** Some practical thermal processes and systems: **a** Optical fiber drawing; **b** data center; **c** horizontal chemical vapor deposition (CVD) reactor for thin-film fabrication; **d** vertical impinging CVD reactor

A few practical thermal systems are shown as examples in Fig. 1. Seen here are the fabrication process for an optical fiber, a data center being cooled by chilled airflow, and two configurations, horizontal and vertical flow, of chemical vapor deposition (CVD) reactors for thin-film fabrication. Many of the complexities mentioned above are encountered in these systems. For instance, material properties of glass in optical fiber drawing are strong functions of temperature, combined modes of radiation, conduction and convection operate at various stages in the process, polymers that are non-Newtonian are generally used for the fiber coating process and large changes in preform/glass diameter occur in the draw furnace [4]. The airflow in data center cooling is generally turbulent, the geometry is complicated, and the flow is coupled with the conduction transport in the electronic system [5]. Chemical reactions and varying species concentrations arise in CVD. This involves chemical kinetics, which vary strongly with temperature and concentration [6]. The boundary conditions are generally quite complicated in all cases and combined transport mechanisms have to be considered. Other practical processes have similar complexities and challenges with respect to computational modeling.

## 2 Numerical Modeling

The various thermal processes and systems mentioned earlier and many others similar to these may be modeled and simulated to obtain the results needed for better insight into the basic processes and for system design and optimization. The equations that describe the flow and convective transport are based on the conservation of mass and energy and the force-momentum balance that give rise to the well-known equations for fluid flow and heat transfer. These may be written for a general three-dimensional, time-dependent process with variable properties, as [1, 5]

$$\frac{\partial \rho}{\partial t} + \nabla \cdot (\rho \bar{V}) = 0 \tag{1}$$

$$\rho\left(\frac{\partial \bar{V}}{\partial t} + \bar{V} \cdot \nabla \bar{V}\right) = \bar{F} - \nabla p + \nabla \cdot \left[\mu\left(\nabla \bar{V} + \nabla \bar{V}^T\right)\right] - \frac{2}{3}\nabla(\mu \nabla \cdot \bar{V}) \tag{2}$$

$$\rho C_p\left(\frac{\partial T}{\partial t} + \bar{V} \cdot \nabla T\right) = \nabla \cdot (k \nabla T) + \dot{Q} + \mu \Phi + \beta T\left(\frac{\partial p}{\partial t} + \bar{V} \cdot \nabla p\right) \tag{3}$$

where $\rho$ is density, $T$ is temperature, $t$ is time, $\bar{V}$ is the velocity vector, $\bar{F}$ is body force, $p$ is pressure, $\mu$ is dynamic viscosity, $C_p$ is specific heat at constant pressure, $\beta$ is coefficient of volumetric thermal expansion, $\mu\Phi$ is viscous dissipation, and $\dot{Q}$ is a volumetric heat source arising from chemical reactions, absorbed radiation, etc. The viscous dissipation and pressure work effects are included in the energy equation, Eq. (3), with the last two terms multiplied by $\beta T$ representing the pressure effect. The bulk viscosity is taken as zero, giving the second viscosity coefficient as $-(2/3)\ \mu$

and Stokes' relationships are used for the viscous forces in the momentum equation, Eq. (2).

The preceding equations may be written for different processes and systems, retaining the relevant terms. For instance, the following forms of the equations apply to a wide range of steady flows:

Mass:

$$\nabla \cdot \left(\rho \bar{V}\right) = 0 \tag{4}$$

Momentum:

$$\rho \bar{V} \cdot \nabla \bar{V} = -\nabla p + \nabla \cdot \left(\mu \nabla \bar{V}\right) \tag{5}$$

Energy:

$$\rho C_p \bar{V} \cdot \nabla T = \nabla \cdot (k \nabla T) \tag{6}$$

where $\bar{V}$ is the velocity vector. For a solid region, the conduction equation is used, given in terms of the summation notation, with thermal conductivity of the solid $k$, as

$$\frac{\partial}{\partial x_i}\left(k \frac{\partial T}{\partial x_i}\right) = 0 \tag{7}$$

For conjugate problems, the heat conduction in the solid region and the convection flow in the fluid region are generally solved separately and then coupled at the solid–fluid interface through the boundary conditions, though other approaches have also been developed.

Recirculating flow is of interest in many problems of practical interest, such as environmental flows, fires, ventilation, and cooling systems. The case of data centers was mentioned earlier. Figure 2 shows some of these circumstances, including heat rejection from power plants to a water body or a cooling tower and a room fire. In the case of heat rejection to water bodies like lakes, rivers, cooling ponds and oceans, the recirculation that may short circuit the hot discharge from the power plant to the inlet is of particular concern since it would lower the efficiency of the plant. Also, of considerable importance is the thermal effect of heat rejection on the thermal cycle of the water body itself. This includes temperature rise and variation in the yearly cycle due to heat rejection. These effects could adversely affect the micro-organisms and life existing in the water body.

Depending on the fluid, dimensions, and operating conditions, the continuum approximation may be inapplicable, leading to slip flow or molecular flow [7]. Such a situation arises, for instance, in an electronic component cooled by the microchannel single-phase flow of a coolant [8]. The Knudsen number, which is the ratio of the mean free path of the particles $\lambda$ to the physical length dimension $L$, determines the flow regime and thus the solution strategy. The overall system, on the other

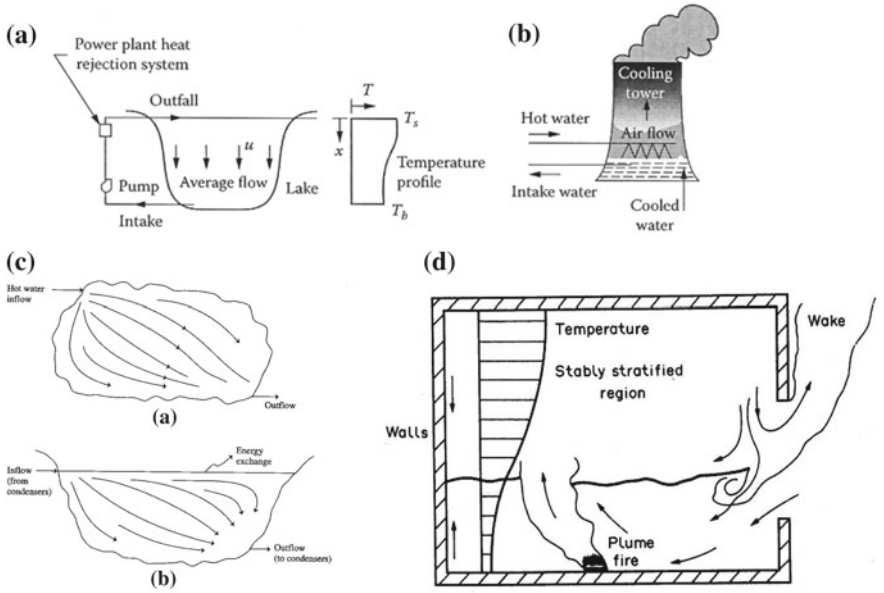


**Fig. 2** **a** Heat rejection to a water body; **b** cooling tower; **c** recirculating flow due to thermal discharge into a lake; **d** room fire

hand, is usually at engineering, or macro-scale, and can be modeled using the usual conservation equations and boundary conditions.

For an important practical process, let us consider the basic characteristics of the optical fiber drawing process, shown in Fig. 1a. The flow of the glass and that of the aiding purge gas in a cylindrical furnace are generally assumed to be axisymmentric. Glass flow is laminar due to the high viscosity and the gas flow is also generally kept laminar to avoid disturbance to the free surface. Then the equations for the glass and the gas are given as [1, 4]

$$\frac{\partial v}{\partial z} + \frac{1}{r}\frac{\partial (ru)}{\partial r} = 0 \tag{8}$$

$$\frac{\partial v}{\partial t} + u\frac{\partial v}{\partial r} + v\frac{\partial v}{\partial z} = -\frac{1}{\rho}\frac{\partial p}{\partial z} + \frac{1}{r}\frac{\partial}{\partial r}\left[r\upsilon\left(\frac{\partial v}{\partial r} + \frac{\partial u}{\partial z}\right)\right] + 2\frac{\partial}{\partial z}\left(\upsilon\frac{\partial v}{\partial z}\right) \tag{9}$$

$$\frac{\partial u}{\partial t} + u\frac{\partial u}{\partial r} + v\frac{\partial u}{\partial z} = -\frac{1}{\rho}\frac{\partial p}{\partial r} + \frac{2}{r}\frac{\partial}{\partial r}\left(r\upsilon\frac{\partial u}{\partial r}\right) + \frac{\partial}{\partial z}\left[\upsilon\left(\frac{\partial v}{\partial r} + \frac{\partial u}{\partial z}\right)\right] - \frac{2\upsilon u}{r^2} \tag{10}$$

$$\rho C_p\left(\frac{\partial T}{\partial t} + u\frac{\partial T}{\partial r} + v\frac{\partial T}{\partial z}\right) = \frac{1}{r}\frac{\partial}{\partial r}\left(rk\frac{\partial T}{\partial r}\right) + \frac{\partial}{\partial z}\left(k\frac{\partial T}{\partial z}\right) + \Phi + S_r \tag{11}$$

Here, $u$ and $v$ are the velocity components in the axial and radial directions, $z$ and, $r$, respectively, $p$ is the local pressure, $T$ the temperature, $t$ the time, $\upsilon$ the kinematic viscosity, $\Phi$ is the viscous dissipation term, and $S_r$ is the radiation source term. The gravitational force term is not included in these equations since its effect is negligible in glass flow. However, the gravitational force is considered for determining the neck-down or free surface profile and for obtaining the buoyancy force in the gas flow, resulting from a combination of the gravity force and the pressure term, as discussed later. For glass, the material properties are strong functions of the temperature, composition, and microstructure. Radiation is the dominant mechanism in the heating of the glass preform for fiber drawing.

The variation in the viscosity has a substantial effect on the flow since it varies dramatically with temperature. An equation based on the curve fit of available data for kinematic viscosity $\upsilon$ is written for silica, in S.I. units, as

$$\upsilon = 4545.45 \ \exp\left[32\left(\frac{T_{\text{melt}}}{T} - 1\right)\right] \tag{12}$$

This indicates the strong, exponential variation of $\upsilon$ with temperature. Here, $T_{\text{melt}}$ is the glass softening temperature, being around 1900 K for silica glass. The radiative source term $S_r$ in Eq. (11) is nonzero for the glass preform/fiber because glass is a participating medium. The variation of the absorption coefficient $\alpha$ with wavelength $\lambda$ can often be approximated in terms of bands with constant absorption over each band. Usually, a two- or three-band model is adequate to determine the radiative transport. Even though the fiber diameter is small, being around 125 $\mu$m, the high temperature dependence of the viscosity makes it necessary to calculate the temperature variation across the fiber using a large number of grid points, typically around 50.

The fiber coating process is another important step in the fabrication of optical fibers and must be modeled and simulated accurately to obtain results that can be used to design the coating applicator and choose the operating conditions. Typical coating thicknesses are on the order of 40–50 $\mu$m and are applied to the uncoated fiber or as a secondary coating to a coated fiber. The basic process involves drawing the optical fiber through a reservoir of coating fluid, which is usually a polymer such as an acrylate, with inlet and outlet dyes. The curing process of the acrylate polymer coating material is carried out by ultraviolet radiation immediately after applying the liquid coating. A balance between the forces, such as surface tension, viscous, gravitational, and pressure forces, gives rise to an upstream meniscus at the entrance, as well as a downstream meniscus at the die exit. At high draw speeds, the upper meniscus breaks down, and the air is entrained into the coating. These entrapped bubbles are undesirable since they can lead to stripping of the coating. Pressurized applicators are often used to reduce the shear at the fiber surface and help in establishing a stable free surface flow. The control of the coating characteristics has been of major concern to the optical fiber industry. These aspects are particularly important at high speeds, ranging beyond 20 m/s to enhance productivity, and also for specialty fibers and fibers of different materials, including polymer fibers. The physical properties of the polymer coating materials, particularly the viscosity, are

of primary importance in the coating process. Surface tension has a significant effect on the shape, stability, and other characteristics of the interface, as discussed later.

Chemical kinetics play a critical role in many important thermal processes such as food extrusion, chemical bonding, and chemical vapor deposition of material from the gas phase. The temperature and concentration of the chemical species in the CVD reactor affect the chemical kinetics, which in turn affects the deposition. In some cases, the process is limited by the chemical kinetics, implying that the transport processes are quite vigorous, and the deposition is restricted largely by the kinetics. It is limited by the transport processes in some other cases. The chemical kinetics for depositing several materials is available in the literature. For instance, the chemical kinetics for the deposition of silicon from silane ($SiH_4$) with hydrogen as the carrier gas in a CVD reactor is given by the expression [9]

$$\hat{K} = \frac{K_o p_{SiH_4}}{1 + K_1 p_{H_2} + K_2 p_{SiH_4}} \tag{13}$$

where the surface reaction rate $\hat{K}$ is in mole of Si/m$^2$s. The parameter $K_o = A \exp(-E/RT)$, $E$ being the activation energy, and $A$, $K_1$, and $K_2$ are constants which are obtained experimentally. The $p$'s are the partial pressures of the two species in the reactor. However, the chemical processes are typically much more complicated, with several intermediate reactions in the gaseous phase and several at the surface. This is particularly true for the deposition of SiC and GaN in metal-organic reactors (MOCVD), as seen later.

## 3 Typical Results and Discussions

Several practical processes have been described in the preceding, along with some of the major complexities faced in obtaining an accurate simulation. These challenges are considered in greater detail here, along with examples and results.

### *3.1 Variable Material Properties and Characteristics*

The accuracy of the results obtained from numerical simulation is a strong function of the material properties used. As mentioned earlier, in most practical processes, properties vary with the local conditions like temperature, pressure, and changes in the material during the process. Unfortunately, accurate property data are often not available at the conditions of the process. This is particularly true for optical fiber drawing where the process is strongly influenced by the temperature-dependent physical properties of silica glass. The radiation properties, such as the variation of the absorption coefficient $\alpha$ with wavelength $\lambda$, have been experimentally obtained

for certain compositions and glasses. But these data are often available only at room temperature, whereas the process occurs at much higher temperatures. Also, data may not be available for the particular glass or composition that is being simulated. Dopants such as rare earth materials are often used to modify the transmission characteristics and for specialized applications. Even though accurate models may be developed for the process, considering different materials and configurations [10], the data on the effect of the dopants on viscosity and on radiation properties are very limited [11]. Some typical data are shown in Fig. 3 and results obtained on optical fiber drawing using these property data are presented later.

Similarly, properties of the coating fluid are important and their variation with temperature is needed for an accurate simulation. The fluids are generally non-Newtonian and large material property changes occur with temperature [12], as shown qualitatively in Fig. 4. The fluid viscosity is often taken as

$$\mu = \mu_o(\dot{\gamma}/\dot{\gamma}_o)^{n-1} \exp(b/T) \tag{14}$$

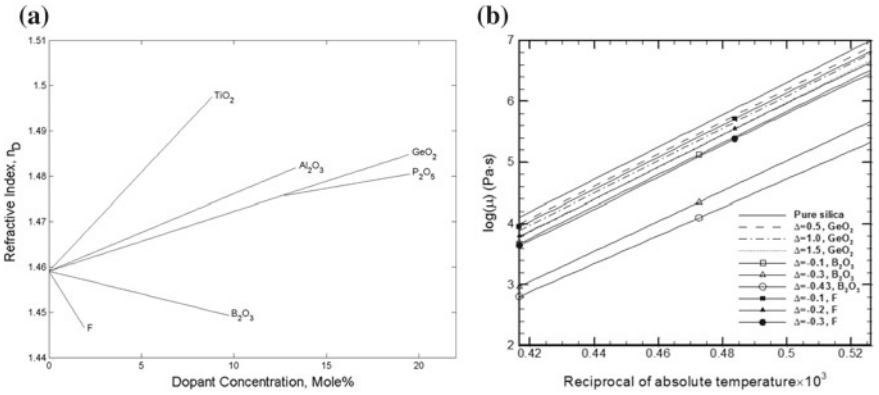


**Fig. 3** Effect of various dopants on the refractive index and viscosity of silica glass in the optical fiber drawing process

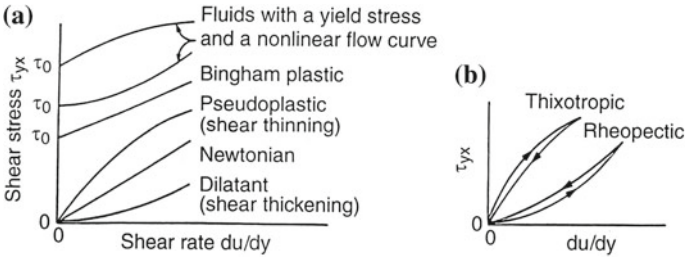


**Fig. 4** Shear stress variation with shear rate for purely viscous, nonelastic, non-Newtonian fluids. **a** Time-independent, and **b** time-dependent fluids [12]

where $\dot{\gamma}$ is the total strain rate, $b$ the temperature coefficient of viscosity, subscript $o$ indicates reference conditions, and $n$ is the power-law index of the fluid. The coating material is thus treated as a generalized Newtonian fluid [13]. Other rheological models may also be used, depending on the fluid. Similar models are used for polymers such as polyethylene and polystyrene in extrusion, injection molding, die flow, and other polymer processing systems. For food extrusion, chemical conversion occurs and the dependence of the viscosity on the degree of conversion is included [14]. Viscoelastic effects, which involve elastic behavior of the material, are also considered in most food processing applications.

Similarly, chemical kinetics play a critical role in chemical vapor deposition and food processing. Simple equations like the one given earlier for Silicon are generally not available or applicable for the wide variety of materials of practical interest. A large number of chemical reactions in the gases and at the deposition surface have to be solved in most cases. The results are strongly affected by the material properties and by the chemical kinetics employed. Lack of accurate property data is clearly a major hurdle in obtaining accurate simulation results in this case.

Besides temperature, pressure, and concentration, the material properties are also often sensitive to the conditions under which the material is stored, as well as the fabrication process, age, and raw materials used. The properties can also change with time, resulting in different values for experiments done at different times. This is of particular concern with biological materials, polymers, and chemicals. Therefore, it is important to know what material and under what conditions it is being employed so that the appropriate properties can be used in the simulation. If possible, properties may be measured as part of the experiment or the simulation for more accurate inputs. Interpolation is employed with available data to obtain the best estimate of the properties under the operating conditions.

Since variable properties arise in many of the processes mentioned here, it is necessary to develop strategies to take these variations into account. In many cases, the variation with temperature, pressure, or other local conditions is so strong that very fine grids are needed to accurately model the process. In transient problems, properties at the previous time step or extrapolated from previous known values are used to avoid iteration at a given time step. Similarly, in steady-state transport, the values at the previous iteration or extrapolated ones are used. The extrapolation approach is similar to the one used by Patankar and Spalding [15] for simulating boundary layer flows.

## *3.2 Verification and Validation*

It is necessary to use simplifications and idealizations in the modeling of practical thermal processes to enable numerical predictions with available or affordable computational resources. Therefore, it is important to verify and validate the mathematical and numerical models to ensure that the results obtained are applicable, realistic, and accurate. It is critical to ensure that the numerical method accurately

solves the equations obtained from the mathematical model. This aspect, known as *verification*, involves grid refinement and varying the arbitrarily chosen parameters, such as convergence criteria and computational domain boundaries, to ensure that the results are essentially independent of the values chosen. *Validation* involves ensuring that the mathematical model is an accurate representation of the physical problem [16]. Among the approaches used is a consideration of the physical behavior of the system, comparisons with available analytical and numerical results, including benchmark solutions, and comparisons with available experimental data on existing similar systems.

Because of the critical importance of verification and validation, extensive efforts are often made to obtain experimental data, whenever possible, for use as checks on numerical predictions. In some cases, a separate, well-designed, experimental setup may be needed to achieve this. For instance, in the modeling and simulation of single and twin-screw polymer extruders, a specially designed cam-driven thermocouple system was developed to obtain the temperature profile in the rotating screw. Also, two rotating cylinders were used to study the mixing phenomena and thus validate the model for twin-screw extrusion. Further details on the various strategies used to validate models for polymer extrusion are given in Ref. [17].

As mentioned earlier and shown in Fig. 1a for the manufacture of optical fibers, a polymer coating is applied for protection against abrasion and to increase strength. The basic coating process involves moving the fiber through a reservoir of coating fluid, followed by a curing process. At the die exit, the coating material is drawn out with the fiber, forming a downstream meniscus, which influences the coating thickness, uniformity, concentricity, and other characteristics. This meniscus is a free surface whose profile is determined by the forces of gravity, surface tension, shear due to the moving fiber, and external shear due to air. These forces are determined from the calculated flows and the forces acting on a guessed profile. The force imbalance is used to generate an iteration scheme, starting with this guessed profile, till the force balance is satisfied, yielding a converged meniscus [18]. Figure 5 shows the numerical results and compares these with experimental data obtained on an actual, practical, fiber coating system. Glycerin was used as the fluid in the experiment for convenience. As seen here, a good agreement was obtained, indicating the validity and accuracy of the model. Several other similar validation studies in materials processing are presented in Ref. [19]. In the simulation of complex practical processes, it is necessary to make all possible efforts to validate the mathematical/numerical models, even if it means spending considerable time and effort in developing an experimental arrangement to obtain the data needed.

### *3.3 Numerical Imposition of Realistic Boundary Conditions*

The accuracy of the results obtained from any numerical simulation is strongly dependent on the accuracy of the numerical treatment of the boundary conditions. In mathematical modeling, isothermal and uniform heat flux conditions, as well as uniform

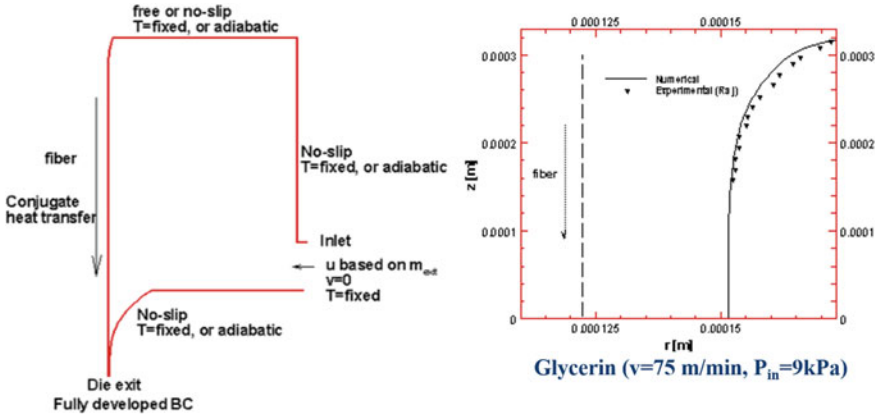


**Fig. 5** Sketch of an optical fiber coating applicator and calculated meniscus at the exit of the die, along with experimental measurements of the profile, for glycerin at a fiber speed of 75 m/min and applicator pressure of 9 kPa

or developed flow conditions at the inlet and outlet, are commonly used to study the basic aspects of the problem. However, such conditions are seldom applicable to practical circumstances. For example, in the modeling of the casting process, with solidification occurring in an enclosed region, the conduction in the walls of the mold is coupled with the transport processes in the solidifying fluid. It is an important consideration that strongly affects the results obtained. The conditions at the inner surface of the mold are not known and the conjugate problem has to be solved to obtain the temperature distribution in the mold as well as that in the solid and the liquid [20]. Numerical solution methods are developed for the solid and liquid regions and continuity of heat flux and temperature at the mold inner surface is employed as the boundary condition. Figure 6a shows the effect of conduction in the mold on the resulting temperature and velocity distributions, as well as on the solidification process. For the casting of metals, alloys, polymers, and other materials, it has been shown in several studies that it is important to model the conjugate transport in the mold walls and in any insulation that may be used in order to obtain realistic and accurate results.

Similarly, in the thermal management of electronic systems, isolated heat sources that approximate components like electronic chips and devices are located on substrates that are conducting. Imposing adiabatic or isothermal conditions on the surfaces is thus not a valid representation of the practical situation. The conduction in the walls distributes the heat input over a larger area of the surface and a concentrated heat source is not a realistic assumption. This conjugate transport results in a substantial effect on the flow and the heat transfer in the electronic system [21]. Figure 6b shows the calculated isotherms and streamlines in an enclosed region with multiple, isolated, heat sources that approximate electronic devices. Clearly, it is seen that the conducting walls play a very significant role in the heat transfer process and must be included in the numerical imposition of the boundary conditions.

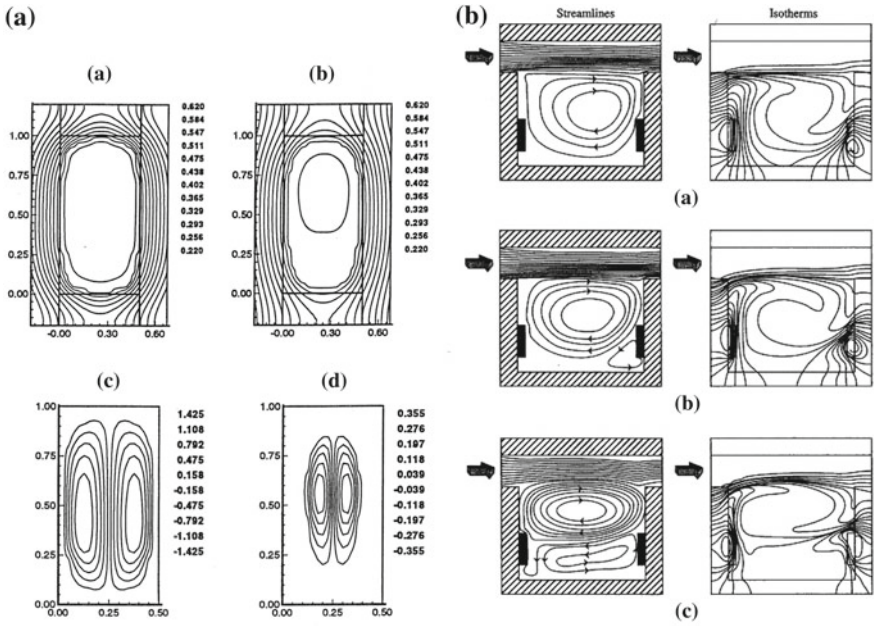


**Fig. 6** Effect of conjugate boundary conditions on the flow and heat transfer in **a** solidification process in casting; and **b** cooling of heat sources representing electronic devices located in an enclosed region

In some practical situations, the boundary conditions are not accurately known. It may be possible to model the entire system, with all its components, to obtain the relevant boundary condition. But this is often difficult in terms of cost and effort. An example of such a circumstance is the optical fiber drawing furnace, where the wall temperature distribution is a critical input needed for simulating the process. This distribution is not easily obtained experimentally because of limited access to the furnace and typically high temperatures that arise. Modeling of the entire system is complicated by the presence of many control and traverse subsystems. To solve this problem, a graphite rod, with thermocouples located at the central axis, was immersed in the furnace, as shown in Fig. 7a. The temperature data thus obtained was employed to solve the inverse problem of determining the furnace wall temperature distribution that would yield the measured rod temperature [22]. Figure 7b shows the measured temperature data in the graphite rod, along with the wall temperature distribution obtained from the inverse calculation. The ends of the heater are water cooled. It is seen that the wall temperature distribution is not significantly affected by the rod size. Inverse calculations do not yield a unique solution. But optimization procedures can be used to minimize the uncertainty in the results obtained, as was also done here. This wall temperature distribution can then be used to accurately simulate the draw process. Other such approaches have been used in practice to obtain the relevant boundary conditions and thus accurately simulate the process.

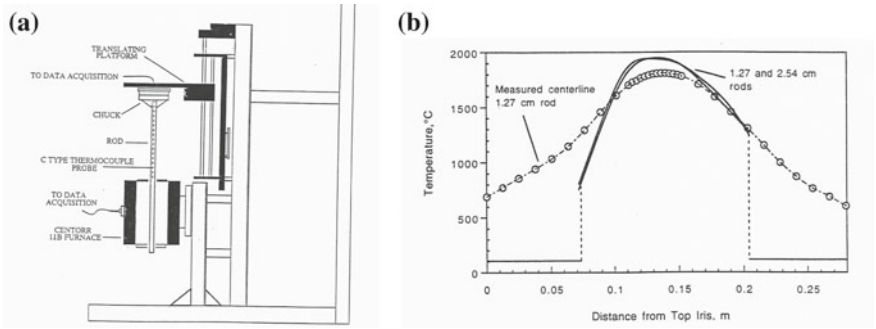


**Fig. 7** **a** Schematic of an experimental system for measuring the temperature distribution in a graphite rod located in an optical fiber drawing furnace; **b** computed furnace wall temperature distributions (solid line) from graphite rod data

## *3.4 Simulation of Recirculating Flows*

There are many other circumstances where recirculating flows such as those shown in Fig. 6 are encountered. The flow in a room due to a fire and the recirculating flow due to heat rejection to a water body were mentioned earlier, see Fig. 2. Because of the importance of these flows, a further discussion on the relevant boundary conditions and on the simulation is needed. Conjugate transport arises in many cases and the conditions similar to the ones outlined in the preceding section are employed. The inlet and outlet flow, as well as temperature distributions are particularly important and must be imposed correctly. Frequently developed conditions are employed at the outlet and uniform conditions at the inlet. The computational domain may also be extended to impose the conditions correctly by considering the region beyond the enclosed space. Spalding and his group carried out extensive simulations of recirculating flows and this work formed the basis for much of the work done on this topic in later years [23].

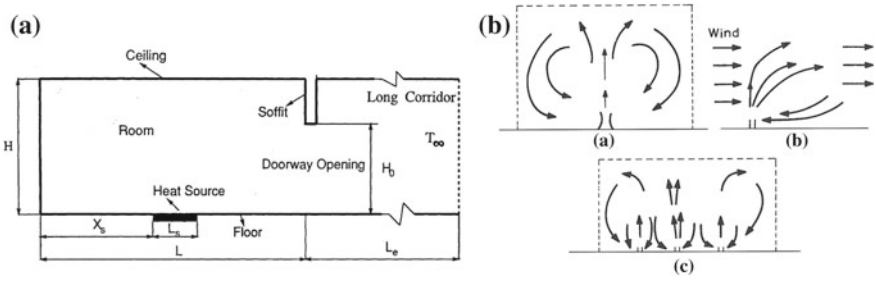


**Fig. 8** **a** Computational domain extension to apply the boundary conditions for flow due to a heat source in a room; **b** recirculating flows in the environment

Figure 8a shows the extension of the computational domain that may be used to apply the velocity and temperature boundary conditions away from the flow region for the circumstance of a heat source in a room. The heat source could be a fire in a room with a doorway opening. Then the boundary conditions are applied at the end of the extended corridor. Typically, developed flow conditions are used, with gradients normal to the opening taken as zero. The temperature of the fluid entering the domain is taken at the outside or ambient temperature, and the temperature gradient of the exiting fluid as zero to ensure negligible diffusion compared to advection (the so-called outflow condition). The extension needed is determined numerically by varying it until the effect on the results is negligible [24]. Figure 8b shows several recirculating environmental flows. The computational boundaries are chosen far from the sources and fluid is allowed to enter and leave the domain, with developed conditions used in most cases.

Figure 9 shows the computed results for two circumstances: flow due to heat rejection into a water body and flow in a channel with two isolated heat sources and a passive vortex generator to enhance the heat transfer. In the first case, the parameter $Gr/Re^2$, where Gr is the Grashof number and Re the Reynolds number, indicates the relative importance of the buoyancy effect. Both Gr and Re are based on inlet

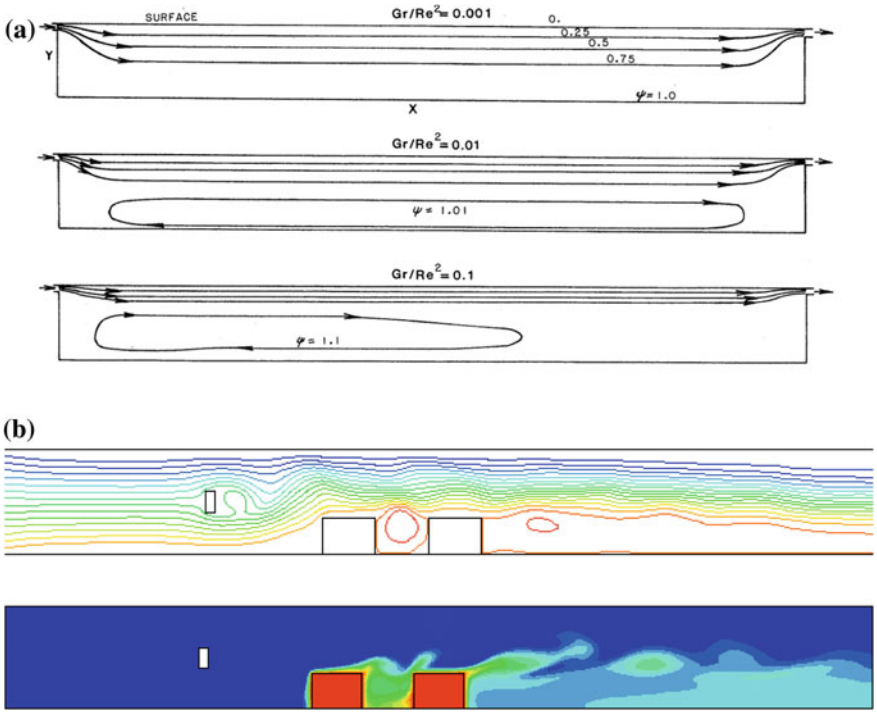


**Fig. 9** **a** Recirculating flow due to thermal discharge into a water body; **b** streamlines and isotherms for flow in a channel with heat sources and a vortex generator

conditions. Therefore, $\mathrm{Gr}/\mathrm{Re}^2 = g\beta\Delta T d/U^2$, where $\Delta T$ is the temperature difference between the inlet and the ambient, $U$ is the inlet velocity, and $d$ is the inlet height. As this parameter increases due to increase in temperature difference $\Delta T$ or decrease in inlet flow velocity, the buoyancy effects increase and reduce the depth of the flow close to the surface and strengthen the recirculation below this top layer. Similarly, in the second case, Fig. 9b, the inflow and outflow conditions may be imposed. The inlet flow and temperature may be taken as uniform and the outflow condition may be imposed at the outlet plane. The inlet conditions may also be applied upstream by employing a domain extension to ensure that the thermal and flow conditions are more realistic. In actual practice, fluid flow at uniform temperature and velocity is generally available not at the inlet but at an upstream location.

## 3.5 *Combined and Complex Transport Mechanisms*

Single transport modes have been studied extensively in the literature. However, most practical thermal processes and systems involve coupled transport mechanisms that complicate the modeling and simulation. Similarly, complex mechanisms like chemical reactions, non-Newtonian fluids, surface tension effects, and free surfaces arise and need to be modeled accurately. Conjugate boundary conditions that involve coupled conduction and convection were considered earlier. Similarly, in the furnace for optical fiber drawing, thermal radiation and convection arise as coupled mechanisms, with conduction in the solid walls, as shown in Fig. 10a. Convection arises

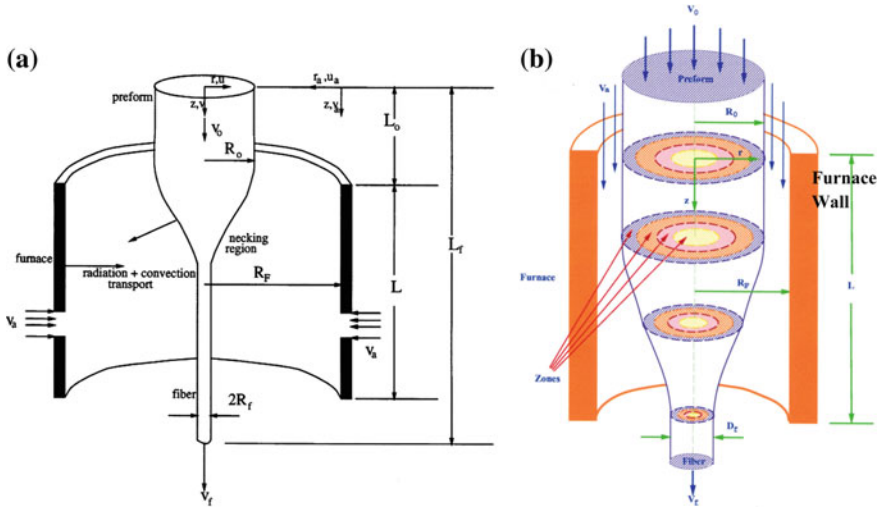


**Fig. 10** **a** Transport mechanisms in the drawing furnace for an optical fiber; **b** axisymmetric finite volume zones for the calculation of radiation in the glass preform and fiber

both in the inert gas environment and in the glass. Beyond the softening point, $T_{melt}$, the glass, which is a subcooled liquid, is treated as a highly viscous liquid, with the viscosity obtained from an equation such as Eq. (12). Below the softening point, the viscosity is quite large, and the behavior is almost like that of a solid. Thermal radiation is the dominant mode of transport for heating up the glass. Radiation models such as the zonal method and the discrete ordinates method may be used to determine the radiation transport in the glass, as well as in the furnace, to obtain the energy absorbed by the preform/fiber, see Fig. 10b. The temperature distribution in the perform/fiber depends on the combined radiation and convection transport and on the viscous dissipation in the glass. The viscous dissipation is particularly important near the end of the neck-down region where the diameters are small and approaching 125 μm [19].

Similarly, forced flow and buoyancy effects arise in different regions of the furnace and the fiber in the drawing of hollow fibers, as shown in Fig. 11. The flow in the fiber core is largely driven by buoyancy and the shear imparted by the moving fiber.

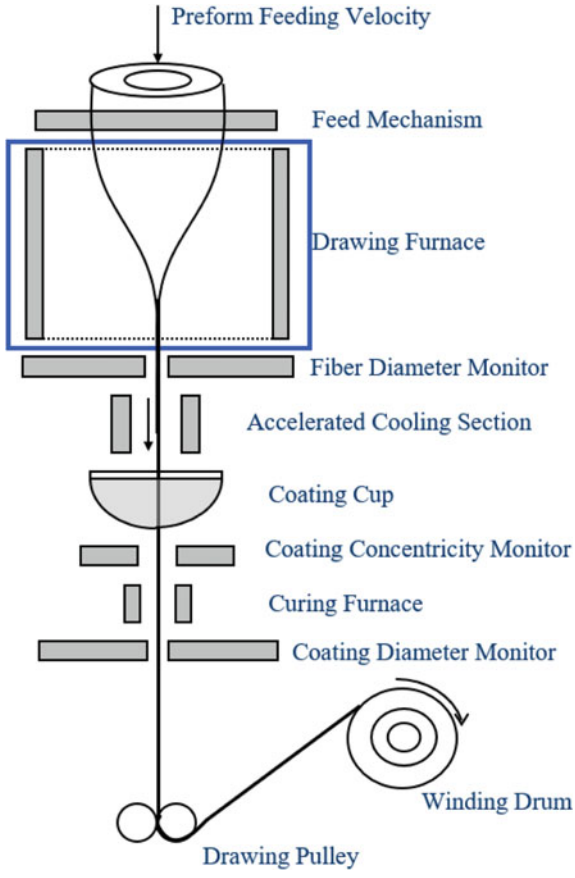


**Fig. 11** Sketch of the optical fiber drawing process for hollow fibers

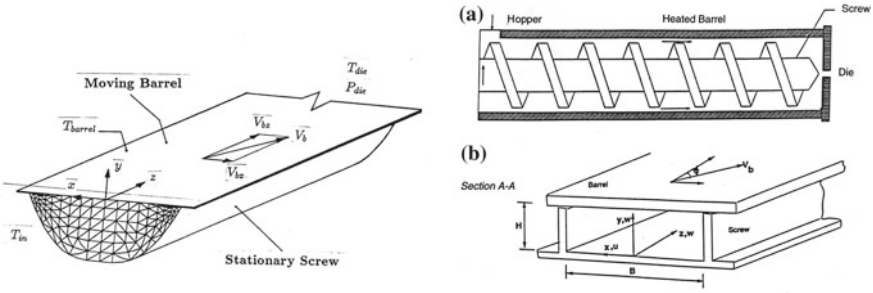


**Fig. 12** A practical single-screw extruder, an idealized extruder; and a simplified model of the resulting channel flow

Thus, the models must include the combined mechanisms to determine the resulting transport, temperature variation, and the flow, as well as the free surface profile as the fiber is drawn from a cylindrical preform of several centimeters in diameter to the fiber diameter of 125 μm.

Another important practical system that may be considered is the screw extrusion process for plastics, including reactive polymers like food materials. Figure 12 shows a sketch of a practical single screw extruder, a simplified version with a rectangular screw profile and a mathematical model, with the coordinate axes located on the rotating screw and the curvature effects being neglected, to yield a simple channel flow. The barrel is then represented by a lid moving at the screw angle. The transport processes involve convective combined heat and mass transfer, conduction in the walls and the screw, and chemical reactions for a reactive material. The resulting product depends on the inlet conditions and imposed concentration $C$ and the temperature $T$. The basic equations thus involve the flow equations, along with the energy and mass transfer equations. Chemical reactions occur and give rise to source terms in the energy and mass conservation equations. The properties vary with concentration and the temperature. The viscosity varies with the shear rate for the non-Newtonian materials typically encountered, as given by Eq. (14).

It is important to model the different transport mechanisms accurately and to ensure that the coupling effects are not neglected. For instance, in combined heat and mass transfer, the Soret and Dufour effects may not be negligible and may need to be included. A typical set of results in the channel flow of a single screw extruder is shown in Fig. 13. The Reynolds numbers are typically much less than one due to the large fluid viscosity so that the diffusion terms are much larger than the convection terms. However, viscous dissipation is important and heats up the polymer as it moves through the channel and the die, as seen from the temperature distributions. It is seen that there is very little mixing going on in the flow. Consequently, various strategies such as gaps in the screw, reverse elements, and different screw profiles are used to enhance mixing. Also, twin-screw extruders have been developed and are increasingly being used because of their superior mixing characteristics.

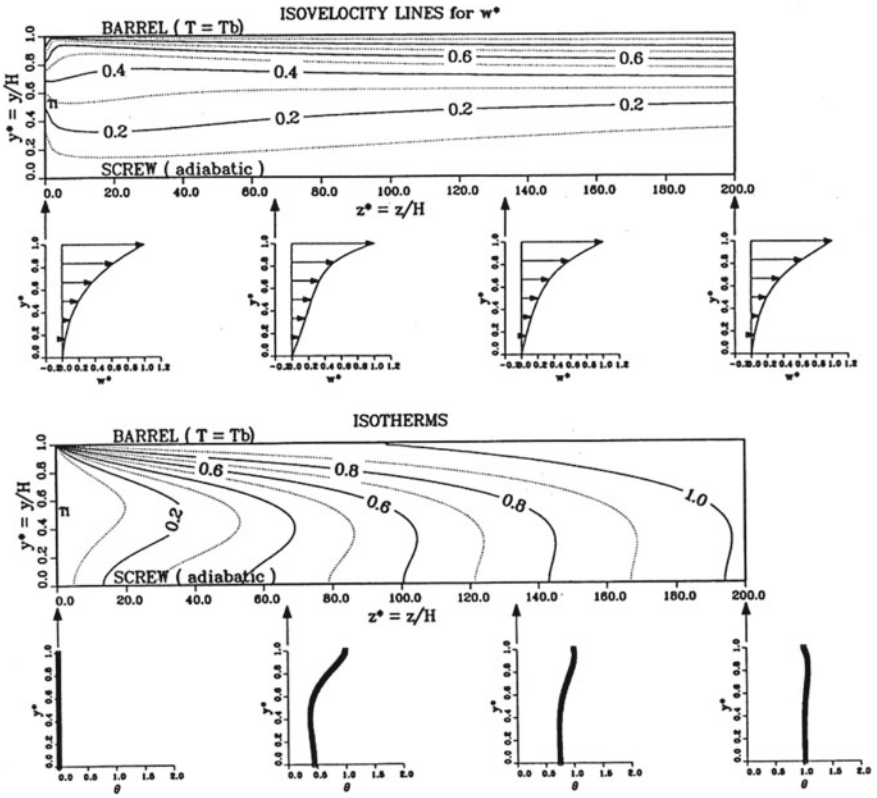


**Fig. 13** Calculated velocity and temperature fields in the extruder at power-law index $n = 0.5$ and dimensionless throughput $qv = 0.3$

Several significant additional effects, such as buoyancy, surface tension, chemical conversion, complex domains, and free surfaces, that considerably complicate the transport phenomena being modeled are encountered in various practical thermal processes. The free surfaces that arise during fiber drawing and the menisci obtained in the coating process have been considered earlier. In these cases, the resulting shape of the free surfaces is governed by a balance of the forces due to shear, tension, gravity, and surface tension. Similarly, a force balance is used at interfaces in multilayered fibers, along with the conservation principles, to determine the resulting profiles.

In the drawing of hollow optical fibers, which are used for applications such as power delivery, sensors, and infrared radiation transmission, a major concern is the collapse of the central core. *A* collapse ratio *C* is defined as

$$C(z) = 1 - (R_1(z)/R_2(z))/(R_{10}/R_{20}) \tag{15}$$

where $R_1$ and $R_2$ are given in Fig. 14b. Thus, $C$ is zero when the radius ratio of the final fiber equals the initial radius ratio, and $C$ is 1 when the central cavity is

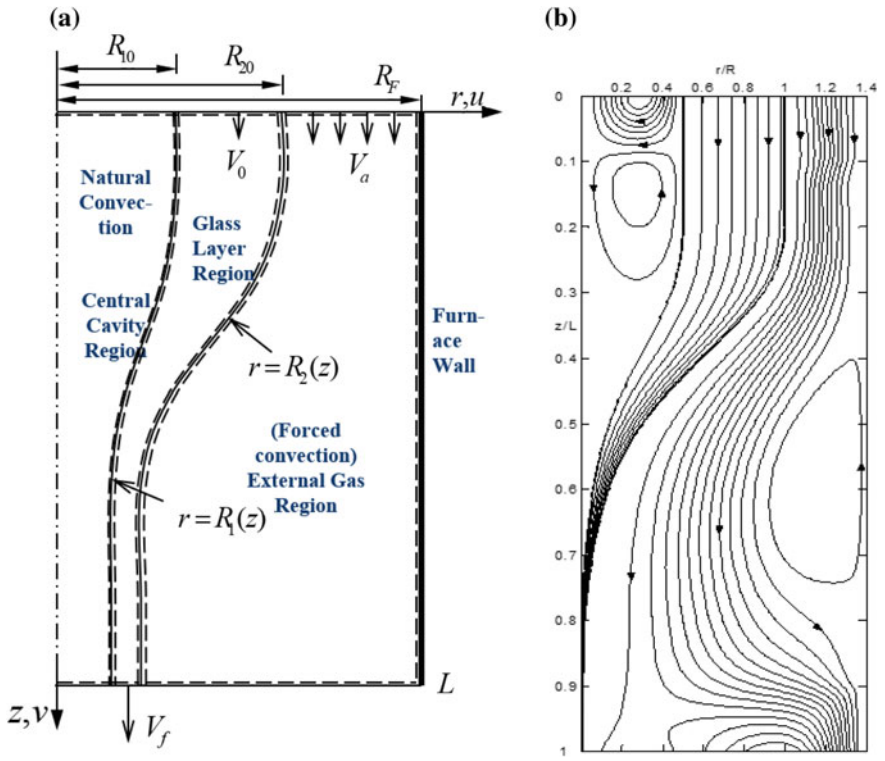


**Fig. 14** **a** Schematic of the furnace for the drawing of a hollow optical fiber; **b** typical streamlines in hollow optical fiber drawing

closed. The effects of the feeding speed of the glass preform, fiber drawing speed, and the furnace temperature on collapse ratio have been studied in detail [25, 26]. Figure 14b shows the calculated streamlines in a typical drawing process, indicating the outer and inner free surfaces of the hollow fiber. Because of the small dimensions of the core, surface tension effects are important and play a very significant role in the collapse. Pressurizing the inner core can also be used to affect the collapse. Figure 15 shows the variation of the collapse ratio $C$ with pressure in the core and with the furnace temperature. It is found that in order to avoid the collapse of the central cavity, we can increase the drawing and feeding speeds, decrease the furnace temperature, or increase the preform outer to inner radius ratio. It is seen that the collapse ratio decreases with a decrease in the pressure difference. This is because higher pressure in the central cavity tends to prevent a collapse of the central cavity.

Thus, a wide variety of additional effects often arise in practical processes and complicate the transport phenomena being modeled. It is necessary to consider all the additional effects that arise and to carry out a detailed scale analysis to determine which ones need to be retained. Then the complex process, with the appropriate additional effects, can be modeled. It must also be noted that Professor Spalding and

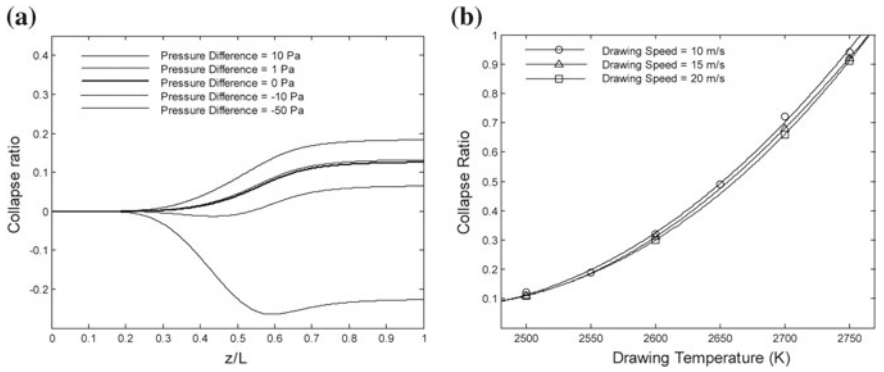


**Fig. 15** Variation of the collapse ratio $C$ in the hollow optical fiber drawing with **a** pressure in the inner core and **b** with furnace temperature

his group studied a wide range of practical problems with concerns similar to those discussed here, paving the way for further research on new and emerging complex problems.

## *3.6 Multiple Length and Time Scales*

A common challenge that arises in the modeling of thermal systems is the presence of different length and time scales in the transport processes. The equations that describe the processes for different scales in the problem are generally different and thus the numerical approaches used for different regions and times may be quite different [26]. For example, consider the numerical simulation of pressure-driven nitrogen flow in long microchannels. Depending on the dimensions of the microchannel, slip flow at the boundaries needs to be considered. Also, conjugate heat transfer arises due to conduction in the walls [8]. Figure 16a shows a sketch of this problem, which is important in many practical circumstances such as those related to the cooling of electronic devices, energy delivery, diagnostics and localized heat input in materials processing systems. For the gas phase, the two-dimensional, axisymmetric or three-dimensional momentum and energy equations are solved, considering variable properties, rarefaction, which involves velocity slip, thermal creep and temperature jump, compressibility, and viscous dissipation. For the solid region, the energy equation is solved with variable properties. Therefore, the two regions are treated with different equations and solution strategies. Figure 16b, c show typical results obtained for different solid, or substrate, materials, including commercial bronze, silicon nitride, pyroceram, and fused silica. The effects of substrate conduction, thermal conductivity, and thickness are clearly seen. It was found that substrate conduction leads to a flatter bulk temperature profile along the channel length, lower maximum temperature, and lower Nusselt number. The effect of substrate thickness

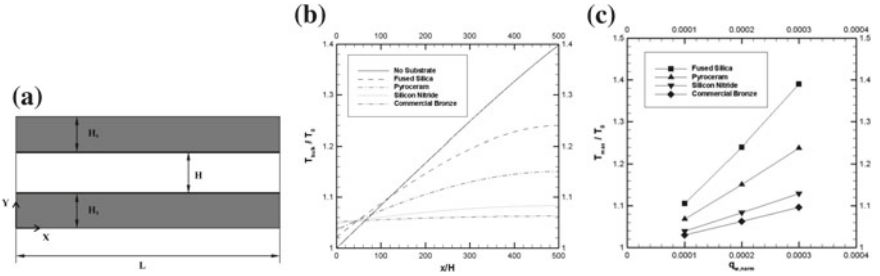


**Fig. 16** Nitrogen flow in a microchannel, with conjugate transport in the walls. **a** Sketch of the microchannel; **b** bulk temperature distribution for different wall materials; **c** maximum temperature as a function of the heat input for different wall materials

is quite similar to that of the material thermal conductivity. That implies that, in terms of thermal resistance, an increase in substrate thickness has a similar effect as that caused by an increase in its thermal conductivity.

The characteristics and quality of the material being processed in manufacturing are generally determined by the transport processes that occur at the micro- or nanometer scale in the material. Examples of this are regions close to the solid–liquid interface in casting or crystal growing, over molecules involved in chemical reactions in chemical vapor deposition and reactive extrusion, or at sites where defects are formed in an optical fiber. On the other hand, engineering aspects are generally concerned with the macroscale, involving much larger dimensions, systems and appropriate boundaries. The operating conditions, for instance, are imposed on boundaries that are typically in centimeter or meter scale. Therefore, different length scales arise and need to be solved by different methodologies, ultimately coupling the two to obtain the overall behavior. Similarly, different time scales arise. For instance, chemical reactions, fluid flow, and thermal diffusion occur at very different time scales.

Changes at the molecular level are important in the generation of thermally induced defects in optical fiber drawing. One such defect is the $E'$ defect, which is a point defect generated at high temperatures during the drawing process and which causes transmission loss and degradation of mechanical strength in the fiber. The differential equation for the time-dependent concentration of these defects was formulated by Hanafusa et al. [27] based on the theory of thermodynamics of lattice vacancies in crystals. It was assumed that the E' defects are generated through the breaking of the Si–O band, and, at the same time, a portion of the defects recombine to form Si–O again. Then the net concentration of the defects is the difference between the generation and the recombination. The equation for $E'$ defect concentration was given as [27],

$$v\frac{\mathrm{d}n_d}{\mathrm{d}z} = n_p(0)v\exp\left(-\frac{E_p}{KT}\right) - n_d v\left[\exp\left(-\frac{E_p}{KT}\right) + \exp\left(-\frac{E_d}{KT}\right)\right] \qquad (16)$$

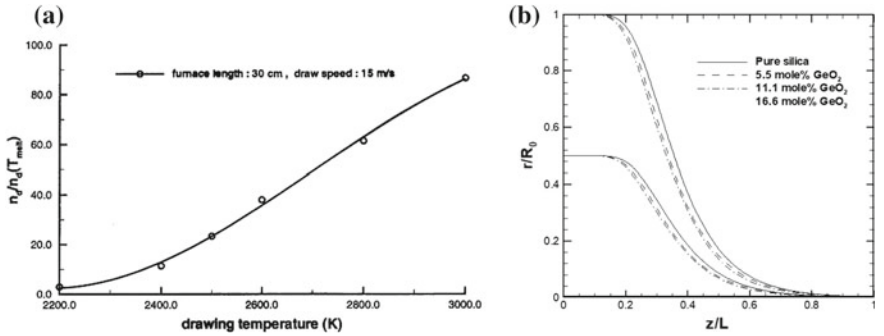


**Fig. 17** **a** Dependence of the average concentration of $E'$ defects on furnace wall temperature in optical fiber drawing; **b** neck-down profile in optical fiber drawing for various $GeO_2$ concentrations in a doped fiber

where $n_d$ and $E_d$ represent the concentration and activation energy of the $E'$ defect; $n_p$ and $E_p$ represent those of the precursors. The initial values and constants are defined by Ref. [27]. Figure 17a shows the dependence of the average concentration of E' defects on the drawing temperature, indicating an increase with temperature, as expected from the higher breakage of the Si–O bond. Figure 17b shows the results on the neck-down profile for a doped fiber, considering different concentrations of the dopant $GeO_2$. Therefore, the defects can be controlled by doping and by varying the operating conditions, particularly the furnace temperature. Several other dopants and operating conditions have been considered in the literature. It was also found that the concentration of the defects is reduced if the drawing is followed by slow cooling, which anneals the fiber and allows the broken bonds to recombine [19].

Another example is provided by reactive thermal processing, such as food and reactive polymer extrusion. In these cases, the microscopic changes in the material are linked with the operating conditions that are imposed on the system. The chemical conversion process is then quantified by chemical kinetics, which depends on the temperature and the concentration [28]. These microscale conversion mechanisms may be coupled with the flow and heat transfer in a screw extruder to obtain the conversion, pressure, and other important quantities. It was shown in Ref. [28] that chemical conversion occurs due to thermal as well as shear effects and the two could be varied to obtain different product characteristics. If the conversion occurs due to shear at room temperature, the product is quite different from that obtained largely by thermal conversion. Thus, by linking microscale behavior with the transport processes, the product and the overall process can be varied.

Multi-scale transport is of interest in environmental flows as well, as shown for a couple of cases in Fig. 18. The heat transfer near the source in a fire or in a polluting system involves much smaller length scales than the transport far downstream. In thermal discharges from power plants and industries, the length scale is of the order of a few meters at the source and of the order or several kilometers far downstream [29]. In room fires, the source may only be a few centimeters, with the room itself

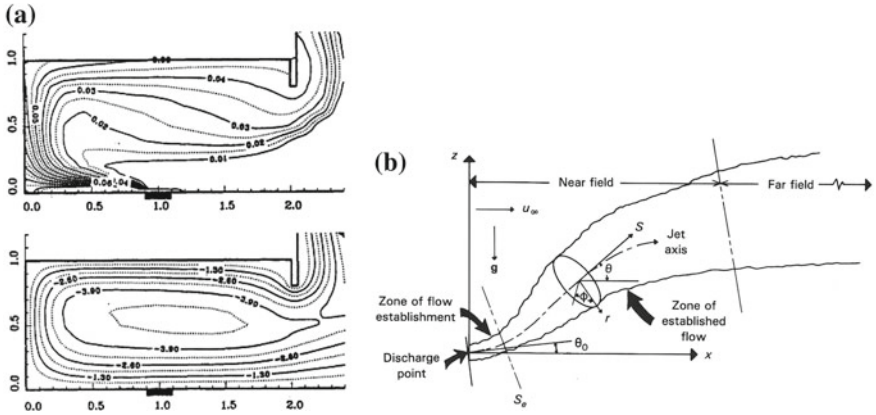


**Fig. 18** Multiple length scales in **a** a room fire and **b** in a thermal discharge into the environment

being several meters in scale. The scales are further apart in large-scale fires as in forest fires. In such cases, the modeling involved, as well as the numerical grid, near the source could be quite different from those far away. For instance, radiation is particularly important near the fire source. But as one moves far away, the flow is dominated by turbulence and buoyancy. Similar considerations apply for heat and material discharges into the environment. Much of the numerical simulation work on such environmental flows has benefited from the extensive research done by Professor Spalding and his group on the modeling of turbulent flow.

## *3.7 Optimization*

Optimization in terms of the operating conditions and the physical design of the system is very important in most practical systems due to global competition. Optimization is carried out with respect to a chosen objective, such as efficiency, cost, production rate, heat transfer rate, and product quality, which is maximized or minimized. For a given physical design, the optimal conditions that yield the best results may be determined. Similarly, the system design may be optimized for the best performance under given conditions. However, multiple objective functions are often of interest. For instance, in the cooling of electronic circuitry, typical design objectives are maximizing the heat removal rate from the components and minimizing the pressure drop. These two objectives can often be treated by considering the two objective functions separately. But the simple approach of combining the objectives into a single function simplifies the problem. Weighted sums may be employed in the development of the combined objective function [30]. However, such a composite objective function is arbitrary, and the results obtained will depend on the way it is formulated.

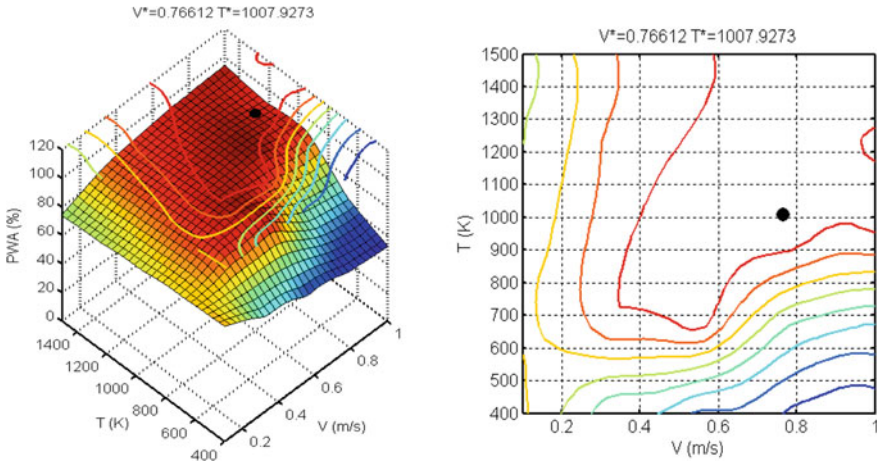


**Fig. 19** Response surface model for PWA and the optimal operating point in a typical CVD process for depositing a silicon film

Lin et al. [31] carried out a detailed study on the design and optimization of chemical vapor deposition (CVD) systems. The main objectives are the deposition rate, which is to be maximized, and the film uniformity, which affects the percentage working area (PWA) that can be used for device fabrication. Results from several computational simulations were obtained to determine the effect of the operating conditions and examine the system performance. Response Surface Method (RSM) models were developed to study the behavior or the response of the system with respect to these variables. The optimization problem was formulated in terms of the RSM models, which were utilized to provide the operating conditions for higher productivity and quality of the film deposited, with a typical result shown in Fig. 19 for PWA in terms of the inlet velocity $V$ and susceptor temperature $T$. The optimum point is shown on the response surface as well as on the contours of constant PWA. In this case, PWA is maximized. However, we could take the deposition rate as the objective function as well and obtain the resulting optimum. Another possibility is to take the acceptable PWA as a constraint and maximize the deposition rate or use an acceptable value of the latter as a constraint and maximize PWA. Some of these results are given in Ref. [19].

If the two or more objective functions that are of interest in a given problem are considered separately and a strategy is developed to trade-off one objective function in comparison to the others, a set of non-dominated designs, termed the *Pareto Set*, which represents the best collection of designs is generated [30, 32, 33]. Then, for any design in the Pareto Set, one objective function can be improved, at the expense of the other objective function. The set of designs that constitute the Pareto Set represent the formal solution in the acceptable design space to the multi-objective optimization problem. The selection of a specific design from the Pareto Set is left to the design engineer. A large literature exists on utility theory, which seeks to provide

additional insight into the decision-making process to assist in selecting a specific design. Many multi-objective optimization methods are available that can be used to generate Pareto solutions. Various quality metrics are often used to evaluate the *goodness* of a Pareto solution obtained and thus improve the method as well as the optimal solution.

The use of this multi-objective optimization approach was demonstrated by Zhao et al. [34] for an electronic system cooling problem, which involved multiple isolated heat sources that represented electronic devices in a channel. Figure 20 shows the response curves separately for the heat transfer rate, given in terms of the Stanton number, $St = Nu/(Re \cdot Pr)$, and the dimensionless pressure drop DP. The former is to be maximized and the latter minimized. Also, shown is the Pareto frontier that may be used to obtain an appropriate design by trading off between the heat transfer and the pressure drop. A higher heat transfer rate is associated with higher pressure drop as well, which is not desirable. Therefore, a designer could choose the best solution for a given application by choosing an acceptable pressure drop for a desired heat transfer rate.

Figure 21 shows another example of multi-objective optimization. Microchannel liquid flows are used for cooling electronic chips. As before, the pressure difference and the heat transfer rate are the main objectives. A detailed simulation is carried out and the non-dominant solutions for the two objectives are used to obtain the Pareto front, given in terms of pumping power and thermal resistance. If a lower

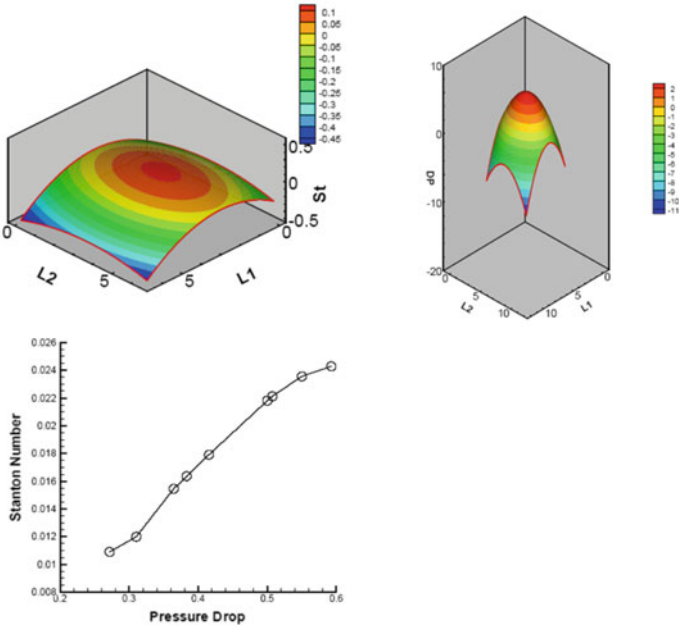


**Fig. 20** Multi-objective optimization with response surfaces for two objective functions St and DP; Pareto Front for selection of optimal design by trade-off between the two objectives

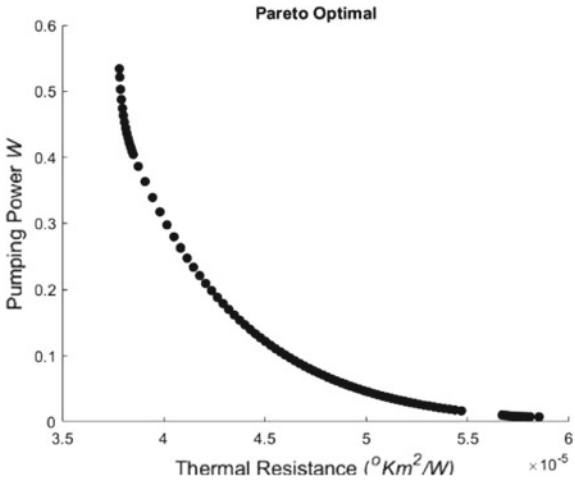


**Fig. 21** Pareto Front for a system for the thermal management of electronic devices by the use of microchannel liquid flow

thermal resistance is desired for higher heat transfer, the pumping power increases. Similarly, for low pumping power the thermal resistance is high and heat transfer is low. From this curve, the best solution may be obtained for a given circumstance using the information on available pumps and costs.

## *3.8 Uncertainties*

Uncertainties arise in the operating conditions and in the hardware in thermal systems. Even if an optimal design is obtained using deterministic conditions and parameters, the uncertainties can lead to unacceptable or unreliable designs. For example, the compositions of the chemical species entering a CVD reactor could have variations on the order of 15%. Similarly, uncertainties exist in inflow rate, susceptor temperature, and rotational speed. Errors may also be encountered in material properties and system dimensions. The rate constants of the chemical reactions may also have significant uncertainties. Several researchers have estimated the randomness of the operating parameters in different systems and processes [35–37].

It can be shown that, due to the existence of the design uncertainties, the traditional deterministic optimization formulation is no longer reliable to generate safe designs because it may lead to a design with a high risk of system failure. Reliability-Based Design Optimization (RBDO) evaluates the probabilities of the system failures and provides a more conservative design which reaches optimality as the failure probabilities that are subject to some acceptable level. Typically, normal distributions of the probabilistic conditions are taken, and an optimal design generated. The productions of the thermal systems are executed based on the optimal design variables. If any design uncertainties are found in the experiments, the simulations, or the mass productions, the information on the uncertainties is fed back to the formulation of

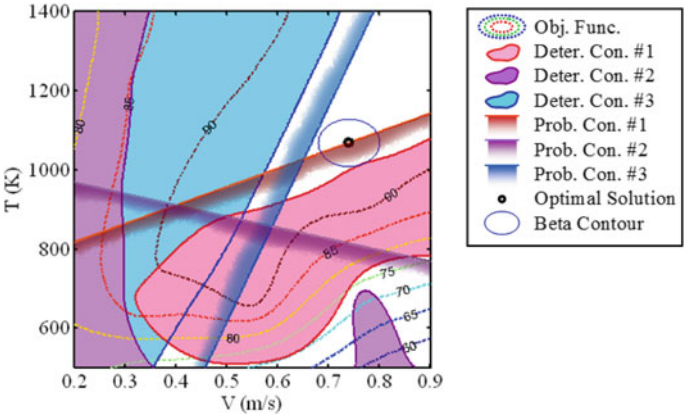


**Fig. 22** Optimization with deterministic design variables and operating conditions, as well as with uncertainties associated with these

the RBDO problems and new optimal conditions can be generated by the proposed strategy. Figure 22 shows the results of the optimization of a CVD system with some deterministic and some probabilistic or uncertainty conditions. The probabilistic constraints are shown as a spread, rather than a deterministic line. The optimum point moves away from that obtained under deterministic conditions [35]. Typically, a failure rate of 0.13% is taken as the acceptable level in reliability-based design. Uncertainties form an important consideration in the design of thermal systems. However, not much has been done so far on this aspect, despite its importance in obtaining realistic and practically useful designs.

## 4 Concluding Remarks

This paper presents several important challenges faced in accurate numerical simulations of practical thermal systems and processes. The paper is a tribute to the extensive work done by Professor D. B. Spalding and his group. This work has provided the basis for meeting many of the challenges discussed in this paper. Among these challenges are variable material properties, that are often treated by employing methods developed by Professor Spalding's group. Similarly, validation of models is a well-known and critical concern in accurate modeling. Accurate imposition of boundary conditions, combined and complex transport mechanisms, uncertainties in the design variables and operating conditions, additional complexities and multiple scales are other challenges that commonly arise and must be addressed. These aspects are considered, along with practical examples where they are of particular importance. Possible approaches to meet these challenges are discussed. Accurate simulation results are needed for studying system behaviour and for design, control,

and optimization. Though only a selected number of practical systems are outlined here, the basic considerations are applicable to a much wider range of problems.

It must be noted that to design and optimize thermal systems and processes, extensive numerical simulations are needed, along with experimental data for validation and physical insight. To obtain accurate simulation results, verified and validated mathematical models and numerical solution methods must be developed, as outlined here. Many books on computational fluid dynamics and heat transfer such as those referenced here, as well as those by Professor Spalding and his group [38, 39] among others, may be used for selecting the algorithm and developing the numerical code. However, a variety of computational software, some of which is based on Professor Spading's work, is commercially available and may be used advantageously to generate the desired numerical results.

**Acknowledgements** The author acknowledges the support of the National Science Foundation, through several grants, and of the industry for the work reported here. The author also acknowledges the interactions with several collaborators and the work done by several students that made it possible to present this review. Finally, the inspiration provided by Professor Spalding is gratefully acknowledged.

## References

1. Jaluria, Y. (2003). Thermal processing of materials: From basic research to engineering. *ASME Journal of Heat Transfer, 125,* 957–979.
2. Jaluria, Y. (2008). *Design and Optimization of Thermal Systems* (2nd ed.). Boca Raton, FL: CRC Press.
3. Bejan, A., Tsatsaronis, G., & Moran, M. (1996). *Thermal design and optimization*. New York: Wiley.
4. Paek, U. C. (1999). Free drawing and polymer coating of silica glass optical fibers. *ASME Journal of Heat transfer, 121,* 774–788.
5. Zhang, J., & Jaluria, Y. (2017). Steady and transient behavior of data centers with variations in thermal load and environmental conditions. *International Journal of Heat and Mass Transfer, 108,* 374–385.
6. Mahajan, R. L. (1996). Transport phenomena in chemical vapor-deposition systems. *Advances in Heat Transfer, 28,* 339–425.
7. Gad-el-Hak, M. (1999). The fluid mechanics of microdevices—The Freeman scholar lecture. *Journal of Fluids Engineering, 121,* 5–33.
8. Sun, Z., & Jaluria, Y. (2010). Unsteady two-dimensional nitrogen flow in long microchannels with uniform wall heat flux,". *Numerical Heat Transfer, 57,* 625–641.
9. Eversteyn, F. C., Severin, P. J. W., Brekel, C. H. J., & Peek, H. L. (1970). A stagnant layer model for the epitaxial growth of silicon from silane in a horizontal reactor. *Journal of the Electrochemical Society, 117,* 925–931.
10. Chen, C., & Jaluria, Y. (2009). Effects of doping on the optical fiber drawing process. *International Journal of Heat and Mass Transfer, 52,* 4812–4822.
11. Izawa, T., & Sudo, S. (1987). *Optical fibers: Materials and fabrication*. Tokyo: KTK Scientific Publishers.
12. Skelland, A. H. O. (1967). *Non-Newtonian flow and heat transfer*. New York: Wiley.
13. Tadmor, Z., & Gogos, C. (1979). *Principles of polymer processing*. New York: Wiley.

14. Kokini, J. L., Ho, C.-T., & Karwe, M. V. (Eds.). (1992). *Food extrusion science and technology*. New York: Marcel Dekker.
15. Patankar, S. V., & Spalding, D. B. (1970). *Heat and mass transfer in boundary layers* (2nd ed.). Intertext: Taylor & Francis, Oxfordshire, UK.
16. Roache, P. J. (1998). *Verification and validation in computational science and engineering*. Albuquerque, New Mexico: Hermosa Publishers.
17. Jaluria, Y. (1996). Heat and mass transfer in the extrusion of non-newtonian materials. *Advances in Heat Transfer, 28,* 145–230.
18. Yoo, S. Y., & Jaluria, Y. (2008). Numerical simulation of the meniscus in the non-isothermal free surface flow at the exit of a coating die. *Numerical Heat Transfer, 53A,* 111–131.
19. Jaluria, Y. (2018). *Advanced materials processing and manufacturing*. Cham, Switzerland: Springer.
20. Viswanath, R., & Jaluria, Y. (1995). Numerical study of conjugate transient solidification in an enclosed region. *Numerical Heat Transfer, 27,* 519–536.
21. Papanicolaou, E., & Jaluria, Y. (1993). Mixed convection from a localized heat source in a cavity with conducting walls: A numerical study. *Numerical Heat Transfer, 23,* 463–484.
22. Issa, J., Yin, Z., Polymeropoulos, C. E., & Jaluria, Y. (1996). Temperature distribution in an optical fiber draw tower furnace. *Journal of Materials Processing and Manufacturing Science, 4,* 221–232.
23. Gosman, A. D., Pun, W. M., Spalding, D. B., & Wolfshtein, M. (1969). *Heat and mass transfer in recirculating flows*. New York: Academic Press.
24. Abib, A., & Jaluria, Y. (1988). Numerical simulation of the buoyancy-induced flow in a partially open enclosure. *Numerical Heat Transfer, 14,* 235–254.
25. Fitt, A. D., Furusawa, K., Monro, T. M., & Please, C. P. (2001). Modeling the fabrication of hollow fibers: Capillary drawing. *Journal of Lightwave Technology*, *19*, 1924–1931.
26. Jaluria, Y. (2009). Microscale transport phenomena in materials processing. *ASME Journal of Heat Transfer*, *131*, 033111-1–17.
27. Hanafusa, H., Hibino, Y., & Yamamoto, F. (1985). Formation mechanism of drawing-induced E′ centers in silica optical fibers. *Journal of Applied Physics, 58*(3), 1356–1361.
28. Wang, S. S., Chiang, C. C., Yeh, A. I., Zhao, B., & Kim, I. H. (1989). Kinetics of phase transition of waxy corn starch at extrusion temperatures and moisture contents. *Journal of Food Science, 54,* 1298–1301.
29. Gebhart, B., Hilder, D. S., & Kelleher, M. (1984). The diffusion of turbulent jets. *Advances in Heat Transfer, 16,* 1–57.
30. Deb, K. (2002). *Multi-objective optimization using evolutionary algorithms*. New York, NY: Wiley.
31. Lin, P. T., Gea, H. C., & Jaluria, Y. (2009). Parametric modeling and optimization of chemical vapor deposition process. *Journal of Manufacturing Science and Engineering, 131*, 011011-1–7.
32. Miettinen, K. M. (1999). *Nonlinear multi-objective optimization*. Boston, MA: Kluwer Acad. Press.
33. Ringuest, J. L. (1992). *Multiobjective optimization: Behavioral and computational considerations*. Boston, MA: Kluwer Acad. Press.
34. Zhao, H., Icoz, T., Jaluria, Y., & Knight, D. (2007). Application of data driven design optimization methodology to a multi-objective design optimization problem. *Journal of Engineering, 18,* 343–359.
35. Lin, P. T., Gea, H. C., & Jaluria, Y. (2010). Systematic strategy for modeling and optimization of thermal systems with design uncertainties. *Frontiers Heat Mass Transfer, 1*(013003), 1–20.
36. Tu, J., Cho, J., & Park, Y. H. (1999). A new study on reliability-based design optimization. *Journal of Mechanical Design, 121,* 557–564.
37. Youn, B. D., & Choi, K. K. (2004). An investigation of nonlinearity of reliability-based design optimization approaches. *Journal of Mechanical Design, 126,* 403–411.

38. Spalding, D. B. (1977). *Genmix: A general computer program for two-dimensional parabolic phenomena*. Oxford, UK: Pergamon Press.
39. Patankar, S. V. (1980). *Numerical heat transfer and fluid flow*. Boca Raton, FL: CRC Press.